The Double Hook

PHILIPPE BARTISSOL AND LEON O. CHUA, FELLOW, IEEE

***Abstract*—This paper describes a new strange attractor exhibited by the same dynamical equations governing Chua's circuit [1], [9] but with a totally different parameter set. The main difference between the new double hook attractor (see the *orange* contour in Fig. 11(a)) and the double scroll is that the vector field of the new attractor has three *real* eigenvalues at the origin, as opposed to the one real and the two complex eigenvalues of the double scroll. We focus on the circuit realization of this attractor and reconcile our experimental observations with theoretical predictions and computer simulations of its structure.**

I. Introduction

The Double Scroll

THE double scroll attractor [2] has been observed in the circuit of Fig. 1(a), whose only nonlinear element is a three-segment piecewise-linear resistor, with $v-i$ characteristic as shown in Fig. 1(b). The dynamics of Chua's circuit are described by

$$\boxed{\begin{aligned} C_1\frac{dv_{C_1}}{dt} &= G(v_{C_2}-v_{C_1})-g(v_{C_1})\\ C_2\frac{dv_{C_2}}{dt} &= G(v_{C_1}-v_{C_2})+i_L\\ L\frac{di_L}{dt} &= -v_{C_2}\end{aligned}} \tag{1.1}$$

where $g(\cdot)$ is the piecewise-linear function in Fig. 1(b), defined by

$$g(v_R)=m_0v_R+\frac{1}{2}(m_1-m_0)|v_R+B_p| + \frac{1}{2}(m_0-m_1)|v_R-B_p|. \tag{1.2}$$

Fig. 2 shows the double scroll attractor [2] observed by solving (1.1) with

$$1/C_1=9,\quad 1/C_2=1,\quad 1/L=7,\quad G=0.7,\quad m_0=-0.5,\quad m_1=-0.8,\quad B_p=1. \tag{1.3}$$

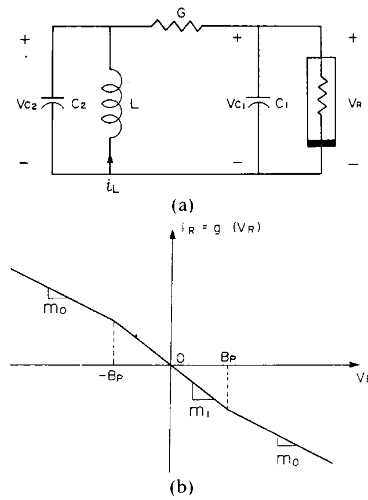

Fig. 1. Chua's circuit. (a) Circuitry. (b) Characteristic of piecewise-linear resistor.

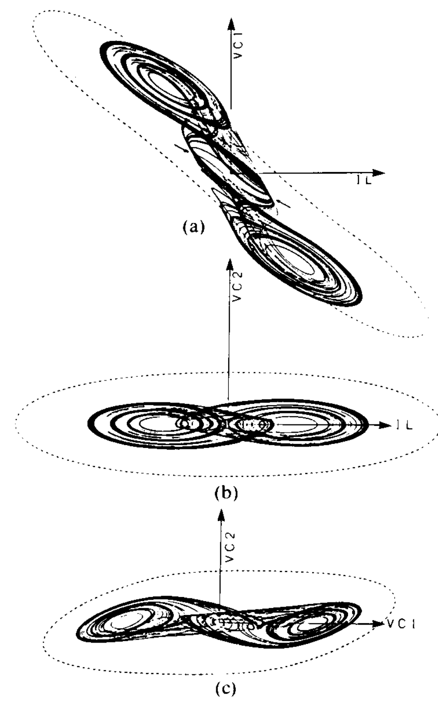

Fig. 2. Double scroll computer simulation. Runge–Kutta integration routine was iterated 10 000 times, with initial conditions: $v_{C_1}(0)=0.15264$, $v_{C_2}(0)=-0.02281$, $i_L(0)=0.38127$. (a) Projection onto the (i_L, v_{C_1})-plane. (b) Projection onto the (i_L, v_{C_2})-plane. (c) Projection onto the (v_{C_1}, v_{C_2})-plane.

Manuscript received August 6, 1987; revised June 2, 1988. This work was supported by the Office of Naval Research under Contract N00014-86-K-0351 and by the National Science Foundation under Grant MIP-8614000. The cost of color printing is supported by a University–Industry grant. This paper was recommended by Associate Editor T. Matsumoto.
P. Bartissol was with the Electronics Research Laboratory, University of California, Berkeley, CA. He is now with the Ecole Nationale Superieure de l'Aeronautique et de l'Espace, Toulouse, France.
L. O. Chua is with the Department of Electrical Engineering and Computer Sciences, University of California, Berkeley, CA 94720.
IEEE Log Number 8823906.

0098-4094/88/1200-1512$01.00

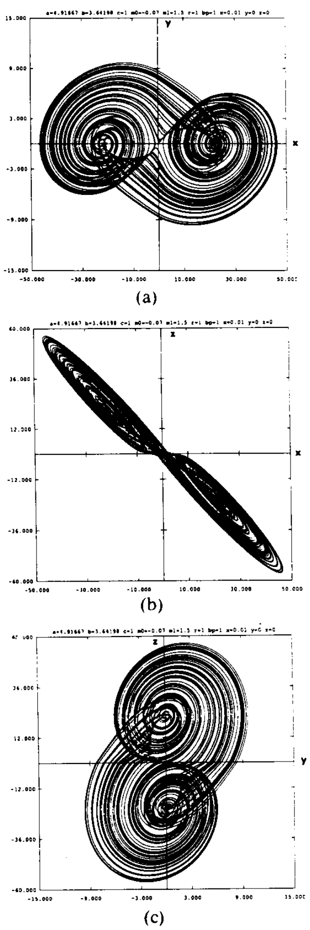

Fig. 3. Computer simulation of the Double Hook dimensionless equations (2.3), associated with the parameter set of (2.6). Runge–Kutta was iterated 10 000 times, with initial conditions: $x_0 = 0.01$, $y_0 = 0$, $z_0 = 0$. (a) Projection onto the (x, y)-plane (or (v, i_{L_2})-plane). (b) Projection onto the (x, z)-plane (or (v, i_{L_1})-plane). (c) Projection onto the (y, z)-plane (or (i_{L_2}, i_{L_1})-plane).2

The Double Hook

The double hook attractor is a new strange attractor displayed by the *same* system (1.1) but with the following parameter values:

$$C_1 \approx -0.0647, \quad C_2 \approx 0.3180, \quad L \approx -0.3005, \quad G \approx 0.539,$$
$$m_0 \approx -0.5013, \quad m_1 \approx -1.3475, \quad B_p \approx 1. \qquad (1.4)$$

The name "double hook" is chosen to call attention to the geometrical structure of the cross section through the origin (see the *orange* contour in Fig. 11(a)), which resembles two oppositely pointed "hooks," joined together on one side.

Fig. 3 shows the new attractor corresponding to this set of parameter values with an appropriate time scaling. This simulation has been obtained by computing the dimensionless form of (1.1).

Note that the most significant difference between the two parameter sets (1.3) and (1.4) is that the circuit giving the new attractor requires a *negative* capacitor and a *negative* inductor.

The realization of such negative devices is not easy.

One technique for synthesizing negative capacitance, or negative inductance, is to use a Negative Impedance Converter (NIC) [3] and a positive-valued capacitance or inductance. One can realize an NIC in two different ways as shown in Fig. 4(a) and (b). In each case, the impedance seen across port 1 is $-(R_1/R_2)Z$.

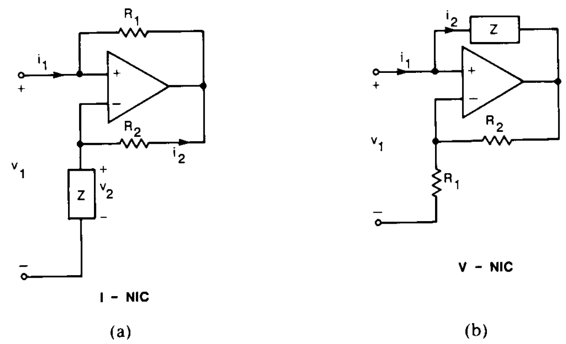

Fig. 4. Negative impedance converter. (a) I-NIC ($V_1 = V_2$, V is unchanged). (b) V-NIC ($I_1 = I_2$, I is unchanged). Let us call Z the impedance of the initial device ($Z = V_2/I_2$) and Z' the impedance of the final device ($Z' = V_1/I_1$). In both, $Z' = -(R_1/R_2)Z$. (Note that if Z is a resistor, there is no difference between an I-NIC and a V-NIC, and if furthermore, $R_1 = R_2$, then $I_1 = I_2$ with the notations of (a).)

However, using NIC's with capacitors or inductors can cause problems. Besides stability and saturation problems, which one can solve respectively by inverting the polarity of the operational amplifiers and scaling the system, one also has to account for the frequency dependent behavior of a real NIC when used with a *dynamical* element, i.e., a capacitor, or an inductor.

II. Physical Realization and Observation

Circuit Realization

In order to avoid the problems associated with the physical realization of negative dynamical elements, we preferred to rewrite the equations in order to obtain a circuit using NIC's exclusively associated with *resistors*, like the one used in obtaining the double scroll, which we reproduce in Fig. 5(a) for convenience. Let us start with (1.1) considering only positive parameter values, so that the equations corresponding to the circuitry of Fig. 1 can be rewritten as follows, with $g(\cdot)$ of (1.2) unchanged:

$$C_1 \frac{dv_{C_1}}{dt} = G(v_{C_1} - v_{C_2}) + g(v_{C_1})$$

$$C_2 \frac{dv_{C_2}}{dt} = G(v_{C_1} - v_{C_2}) + i_L$$

$$L \frac{di_L}{dt} = v_{C_2}. \qquad (2.1)$$

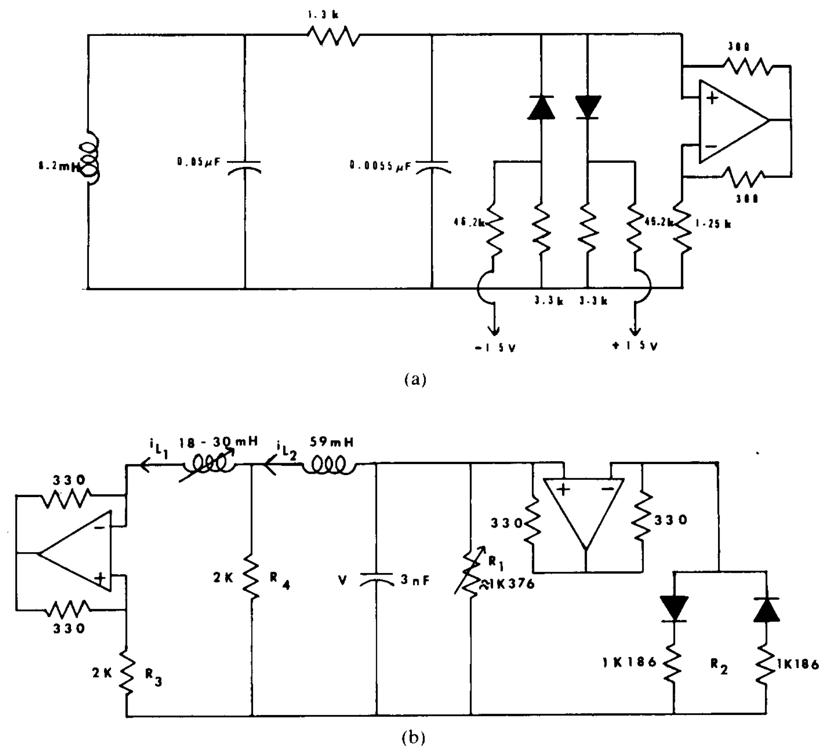

Fig. 5. Chaotic circuits. (a) Circuit for observing the double scroll attractor. (b) Circuit for observing the double hook attractor.

Defining the new variables

$$
\begin{aligned}
i_{L_1} &\equiv i_L\\
i_{L_2} &\equiv G v_{C_2}\\
v_C &\equiv G v_{C_1}
\end{aligned}
\tag{2.2}
$$

and the new parameters

$$
\begin{aligned}
L_1 &\equiv GL\\
L_2 &\equiv \frac{C_2}{G}\\
C &\equiv \frac{C_1}{G}
\end{aligned}
\tag{2.3}
$$

we obtain

$$
\boxed{
\begin{aligned}
C\frac{dv_C}{dt} &= -i_{L_2} - g'(v_C)\\
L_2\frac{di_{L_2}}{dt} &= v_C - R(i_{L_2} - i_{L_1})\\
L_1\frac{di_{L_1}}{dt} &= R(i_{L_2} - i_{L_1}) + R i_{L_1}
\end{aligned}
}
\tag{2.4}
$$

where $R = 1$ and $g'(v_C) \equiv -v_C - g(v_C)$ has the form

$$
g'(v_C) = m_0' v_C + \frac{1}{2}(m_1' - m_0')|v_C + B_p| + \frac{1}{2}(m_0' - m_1')|v_C - B_p|. \tag{2.5}
$$

Note that

$$
\begin{aligned}
m_0' &= -1 - m_0\\
m_1' &= -1 - m_1.
\end{aligned}
\tag{2.6}
$$

Therefore, by a rescaling of the system, the parameter set (1.3) becomes, for the new equations (2.5):

$$
\begin{gathered}
L_1 = 0.162, \quad L_2 = 0.590, \quad C = 0.120, \quad R = 1\\
m_0' = -0.07, \quad m_1' = 1.5, \quad B_p = 1.
\end{gathered}
\tag{2.7}
$$

Since (2.4) with parameter set (2.7) is strictly equivalent to (1.1) with parameter set (1.3), the corresponding attractor is identical to that given in Fig. 3.

Note that the transformed circuit whose dynamics are described by (2.4) with elements defined by (2.5) and (2.7) contains only *positive-valued* dynamical elements. It can easily be built as shown in the schematic of Fig. 5(b).

This circuit requires only two active devices, one negative resistor and one piecewise-linear resistor, both of which can be easily constructed [4], especially because each is grounded at one terminal.

The left op amp is part of an NIC block, which inverts the sign of R_3. The piecewise-linear resistor is located on the right of the capacitor. Note that unlike in [4], the op amp in Fig. 5 is assumed to operate only in the *linear* regime. Here, the two diodes are responsible for realizing the piecewise-linear characteristics in Fig. 6(a).

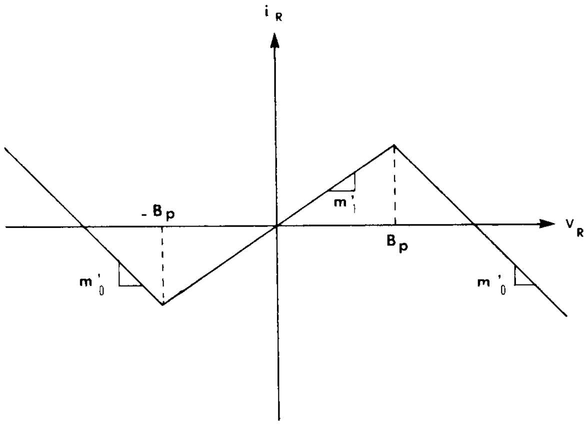

(a)

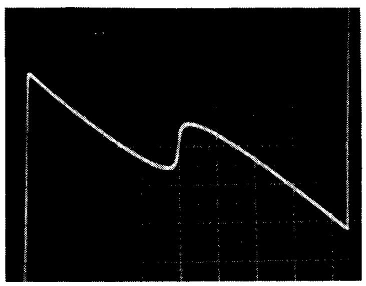

(b)

Fig. 6. Constitutive relation of the nonlinear resistor. (a) Ideal piecewise-linear characteristic. (b) Oscilloscope trace of the actual nonlinear-characteristic. Horizontal scale: 2 V/div. Vertical scale: 0.2 V/div.

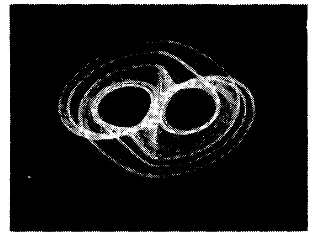

(a)

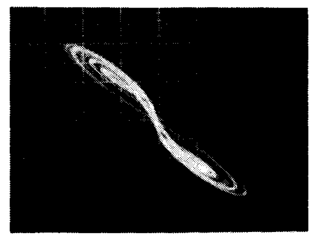

(b)

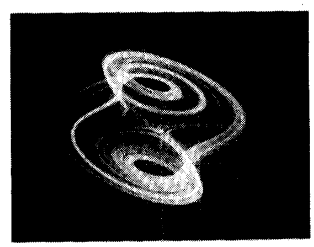

(c)

Fig. 7. Projections of the double hook attractor seen with an oscilloscope, (a) (v_C, i_{L_2})-plane. Horizontal scale: 2 V/div. Vertical scale: 0.4 V/div. (b) (v_C, i_{L_1})-plane. Horizontal scale: 2 V/div. Vertical scale: 2 V/div. (c) (i_{L_2}, i_{L_1})-plane. Horizontal scale: 2 V/div. Vertical scale: 0.4 V/div.

Experimental Observations

After further time scaling and amplitude normalization to ensure that currents and voltages take on reasonable values, the final set of circuit parameter values for (2.4) is

$$L_1 = 16.2\text{ mH},\quad L_2 = 59\text{ mH},\quad C = 3\text{ nF},\quad R = 2\text{ k}\Omega$$
$$m_0' = -0.035\times 10^{-3},\quad m_1' = 0.75\times 10^{-3},\quad B_p = 0.2. \tag{2.8}$$

Fig. 6(a) gives the constitutive relation of the ideal piecewise-linear resistor and Fig. 6(b) shows the actual characteristics measured in the laboratory. The smooth transition of the curve near the breakpoint is due to the use of germanium diodes. As the required breakpoint voltage was so low, we had to use this type of diode, whose threshold is equal to 0.2 V, instead of the more ideal silicon diodes (threshold: 0.6 V). We also had to consider the internal resistance of the diode, in order to obtain suitable values for the nonlinear resistor. The values R_1 and R_2 in Fig. 5(b) can be easily calculated in order to obtain suitable values for m_0' and m_1'. However, since m_0' is very low, the internal resistance of the diodes cannot be neglected. Experimentally, we used a variable resistor for R_1 and tweaked it until we obtained a suitable characteristic on the Negative Resistance Curve Tracer [5] (cf. Fig. 6(b)).

Note that the saturation characteristic of the op amp gives rise to the inevitable eventual passivity in $g'(\cdot)$ (vertical segments in Fig. 6(b)). Unfortunately, the saturation occurs in a region very close to the attractor, i.e., $v_C = 8$ V, while the maximum usable range for v_C in Fig. 6(b) is also about 8 V. In order to prevent the attractor from crossing into this region of operation, we had to adjust further the value of the resistor R_1 in Fig. 5(b).

Fig. 7(a)–(c) shows various projections of the attractor observed from the circuit realization in Fig. 5(b). We were able to observe i_{L_2} by inserting a small series resistance followed by two buffers and a differential amplifier. We measured i_{L_1} by measuring the proportional voltage across R_3 (see Fig. 5(b)).

Fig. 8 shows the same attractor viewed from various perspectives using the 3-D-rotator described in [6]. Each picture represents the projection of the attractor from different positions.

Fig. 9(a)–(l) shows the various attractors that can be physically observed during the bifurcation process by tun-

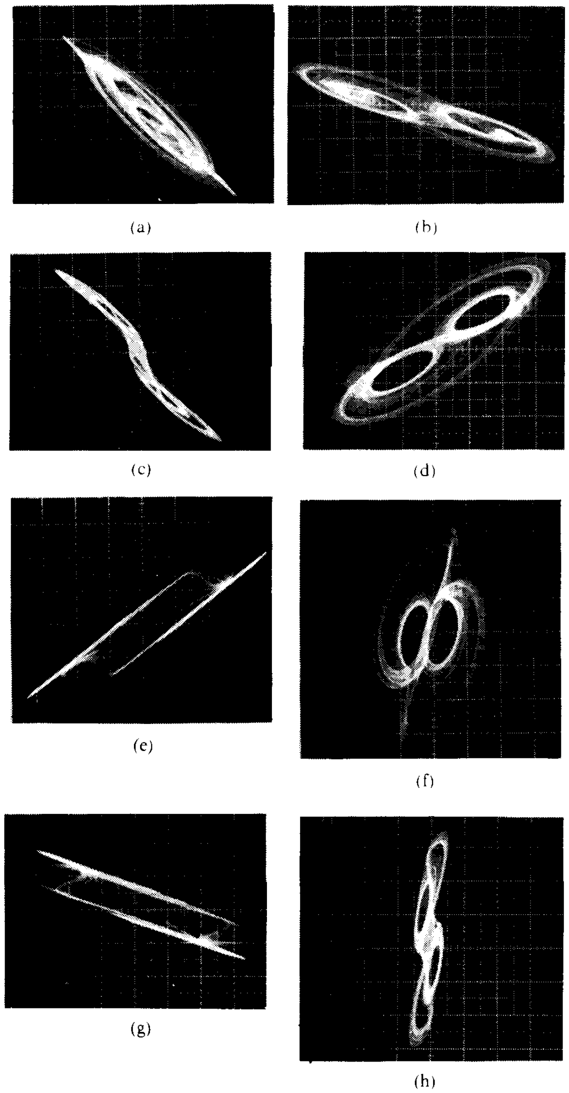

Fig. 8. Various projections of the rotated double hook attractor. (These sometimes surprising pictures give us an idea of the three-dimensional attractor. They all have the same scale and are projections of the double hook along various directions.)

ing L_1. Observe the period doubling from Fig. 9(a)–9(b) and then back to a period 1 limit cycle in Fig. 9(c), i.e., without any further period doublings. This bifurcation phenomenon is clearly different from that which gives birth to the double scroll.

III. Geometric Structure of the Attractor

Dimensionless Form

Recall the dynamics (2.4) and note that the function $g'(\cdot)$ of (2.5) satisfies

$$g'(B_P v_C) = B_p g'(v_C). \tag{3.1}$$

Therefore, by rescaling,

$$x \equiv \frac{v_C}{B_P} \quad y \equiv R\frac{i_{L_2}}{B_P} \quad z \equiv R\frac{i_{L_1}}{B_P}$$

$$\tau \equiv R\frac{t}{L_2} \quad \alpha \equiv \frac{L_2}{R^2 C} \quad \beta \equiv \frac{L_2}{L_1}. \tag{3.2}$$

Equation (2.4) is transformed into the following simpler dimensionless form

$$\boxed{\begin{aligned} \frac{dx}{d\tau} &= \alpha(-y - f(x)) \\ \frac{dy}{d\tau} &= x - y + z \\ \frac{dz}{d\tau} &= \beta y \end{aligned}} \tag{3.3}$$

where $f(x) = Rg'(x)$,

$$\text{i.e., } f(x) = \begin{cases} bx + a - b, & x \geqslant 1 \\ ax, & |x| \leqslant 1 \\ bx + b - a, & x \leqslant -1 \end{cases} \tag{3.4}$$

and

$$a = Rm_1' \quad \text{and} \quad b = Rm_0'. \tag{3.5}$$

Again, Fig. 3 shows the attractor corresponding to (3.3) with the exact parameter set:

$$\tau = t/0.162, \quad \alpha = 0.590/0.120, \quad \beta = 0.590/0.162,$$
$$a = 1.5 \quad \text{and} \quad b = -0.07. \tag{3.6}$$

Note that (3.3) is symmetric with respect to the origin.

To find the equilibrium points, let us solve:

$$\begin{aligned} y + f(x) &= 0 \\ x - y + z &= 0 \\ y &= 0 \end{aligned} \tag{3.7}$$

It follows from (3.7) that the three zeros of $f(\cdot)$ determine the equilibrium points; namely,

$$\begin{cases} P^+ = (k, 0, -k) \\ 0 = (0,0,0) \\ P^- = (-k, 0, k) \end{cases} \tag{3.8}$$

where $k = (b-a)/a$ (with the parameter set of (3.6), $k \approx 22.4$, which, when compared to the breakpoint $B_P = 1$, explains the large size of the attractor).

Due to the nature of the nonlinearity $f(\cdot)$, the space can be divided into three piecewise-linear subsets, each subset including one of the above equilibrium points, as follows:

$$\begin{cases} D_1 \equiv \{(x, y, z) : x \geqslant 1\} \\ D_0 \equiv \{(x, y, z) : |x| \leqslant 1\} \\ D_{-1} \equiv \{(x, y, z) : x \leqslant -1\}. \end{cases} \tag{3.9}$$

In each region D_1, D_0, and D_{-1}, the system (3.3) is linear.

In D_1 and D_{-1}, (3.3) has one real negative eigenvalue:

$$\gamma_P \approx -0.991 \qquad \text{(stable)}$$

and two complex-conjugate eigenvalues:

$$\sigma_P \pm j\omega_P \approx 0.168 \pm j1.112 \qquad \text{(unstable)}.$$

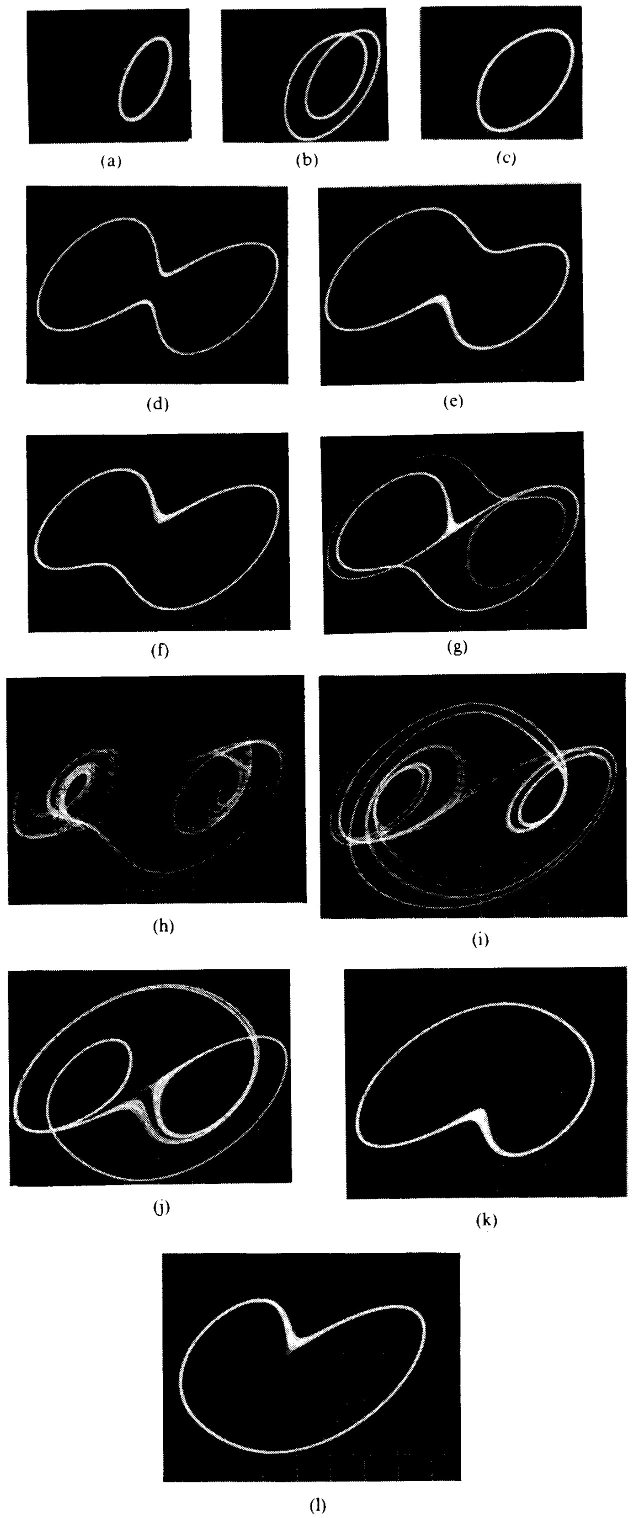

Fig. 9. Closed orbits and chaotic attractors observed near the double hook by tuning L_1 (projections on the (v_C, i_{L_1})-plane). This set of pictures gives an idea of the bifurcation process (our observation terminates after Fig. 9(l) because of saturation in one of the op amps). (a) $L_1 = 28.0$ mH. (b) $L_1 = 24.0$ mH. (c) $L_1 = 21.5$ mH. (d) $L_1 = 20.7$ mH. (e) $L_1 = 20.0$ mH. (f) $L_1 = 19.9$ mH. (g) $L_1 = 19.8$ mH. (h) $L_1 = 19.4$ mH. (i) $L_1 = 19.0$ mH. (j) $L_1 = 18.7$ mH. (k) $L_1 = 18.65$ mH. (l) $L_1 = 18.6$ mH.

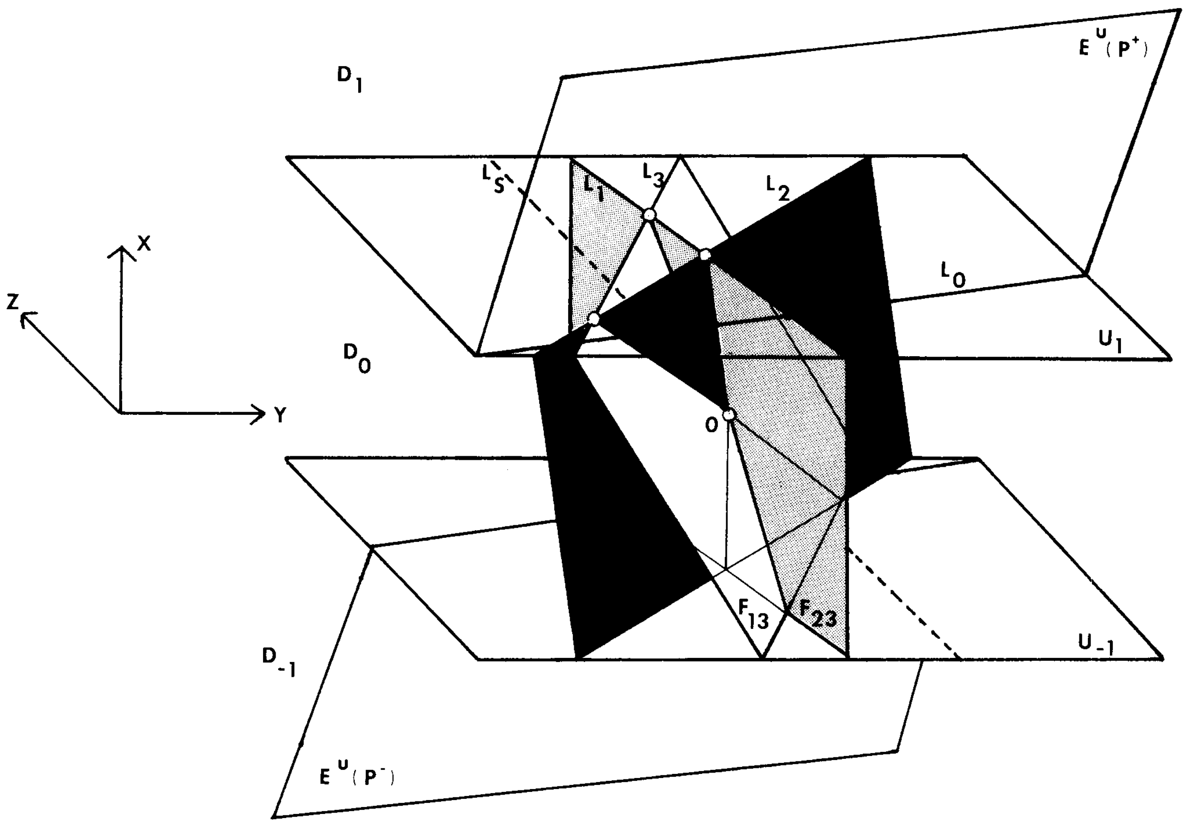

Fig. 10. Relative position of the various subsets.

Three real eigenvalues are associated with region D_0, one positive:

$$\gamma_{01} \approx 1.279 \qquad \text{(unstable)}$$

and two negative:

$$\gamma_{02} \approx -3.310 \quad \text{and} \quad \gamma_{03} \approx -6.344 \qquad \text{(stable)}.$$

Let us examine the structure formed by the principal planes, lines and points, which sustain the attractor.

Geometric Structure

Define (see Fig. 10):

$E^s(P^+)$: *the stable eigenspace of region* D_1 $(Dim = 1)$

$E^u(P^+)$: *the unstable eigenspace of region* D_1 $(Dim = 2)$

$E^{u1}(0)$: *the unstable eigenspace of region* D_1 *associated with* γ_{01} $(Dim = 1)$

$E^{s2}(0)$: *the stable eigenspace of region* D_1 *associated with* γ_{02} $(Dim = 1)$

$E^{s3}(0)$: *the stable eigenspace of region* D_1 *associated with* γ_{03} $(Dim = 1)$

$F_{12}(0)$: *the subset generated by* $E^{u1}(0)$ and $E^{s2}(0)$ $(Dim = 2)$

$F_{13}(0)$: *the subset generated by* $E^{u1}(0)$ and $E^{s3}(0)$ $(Dim = 2)$

$F_{23}(0)$: *the subset generated by* $E^{s2}(0)$ and $E^{s3}(0)$ $(Dim = 2)$

$$U_1 = \{(x, y, z) : x = 1\} = D_1 \cap D_0 \qquad (\text{Dim} = 2)$$

$$U_{-1} = \{(x, y, z) : x = -1\} = D_{-1} \cap D_0 \qquad (\text{Dim} = 2).$$

Lines and points on the plane U_1:

$$L_0 = E^u(P^+) \cap U_1$$
$$L_1 = F_{23} \cap U_1$$
$$L_2 = F_{12} \cap U_1$$
$$L_3 = F_{13} \cap U_1$$
$$L_s = \{(x, y, z) : x = -1 \text{ and } y + f(x) = 0\}$$
$$A = L_0 \cap L_1$$
$$B = L_0 \cap L_s$$
$$C = L_2 \cap L_3$$
$$D = L_1 \cap L_s.$$

Note that L_s clearly separates the plane U_1 into two regions, one where $dx/dt > 0$ (upgoing trajectory) and another where $dx/dt < 0$ (downgoing trajectory).

Let us try to describe the trajectories near U_1, basing the analysis on Fig. 11(a) and (b).

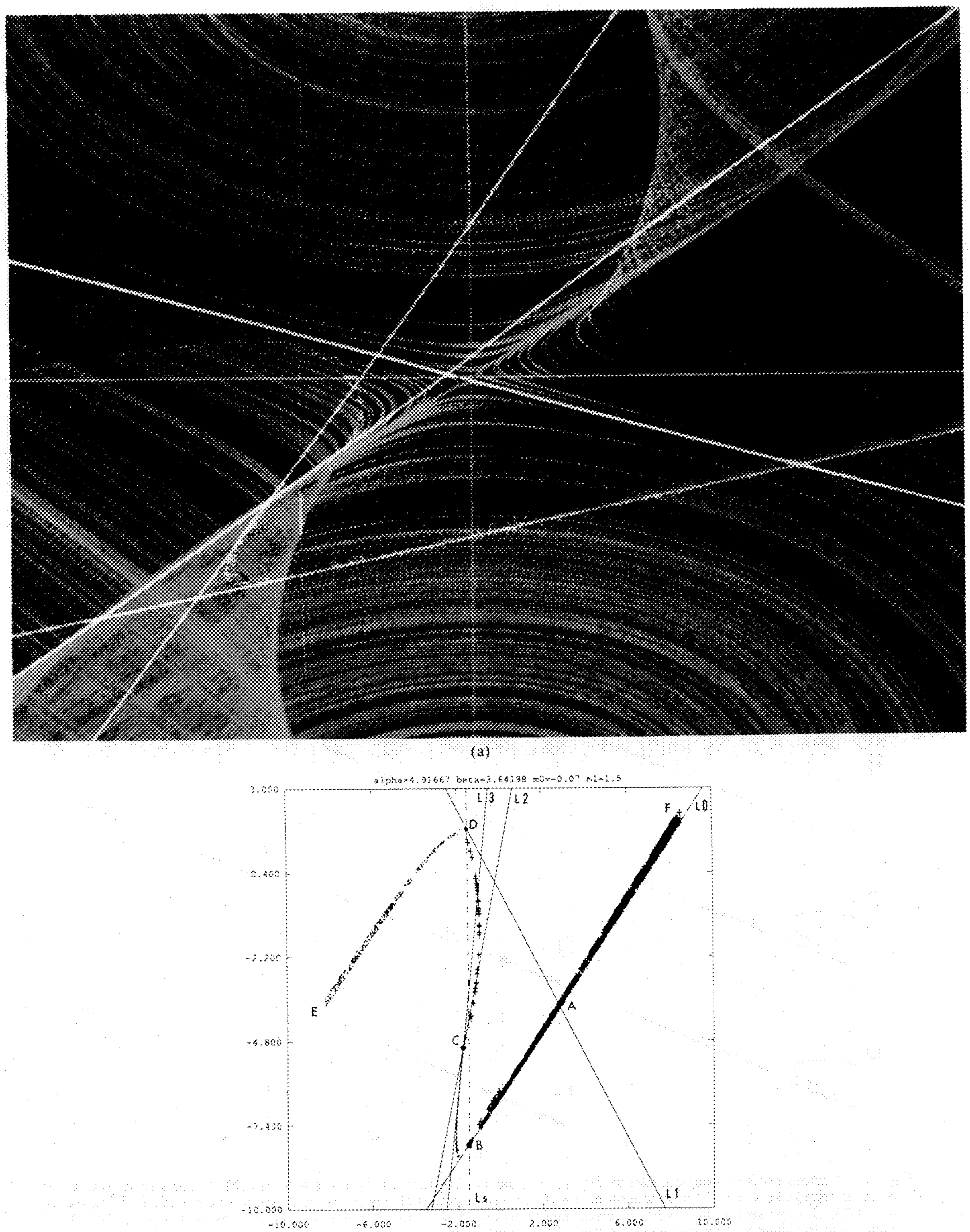

(a)

(b)

Fig. 11. Cross sections at the boundary. (a) Cross section at $x=1$ and projection of the trajectory onto the same plane $x=1$. The points represent upgoing trajectories while the crosses denote downgoing trajectories. The "Z-shape" contour in *orange* is the *double hook* attractor. The blue (resp. green and purple) lines represent the projection of the part of the trajectory located in the upper (resp. middle and lower) region and L_1, L_2 and L_3 are shown in yellow. (b) Cross section at $x=1$ (the points represent upgoing trajectories while the crosses denote downgoing trajectories).

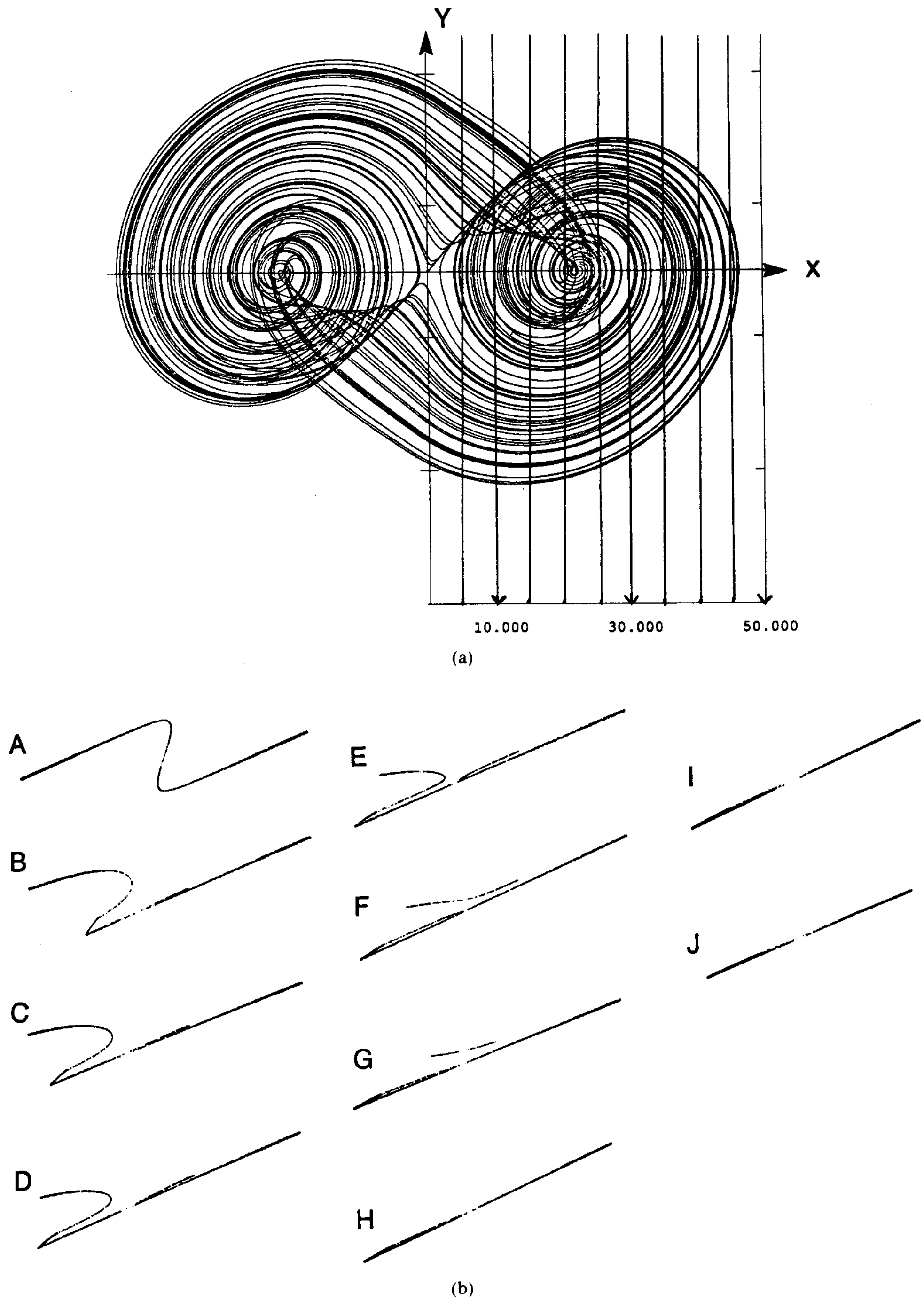

Fig. 12. Various cross sections parallel to the (y, z)-plane. (a) Location of the cross sections. (b) A: cross section at $x = 0$, B: cross section at $x = 5$, C: cross section at $x = 10$, D: cross section at $x = 15$, E: cross section at $x = 20$, F: cross section at $x = 25$, G: cross section at $x = 30$, H: cross section at $x = 35$, I: cross section at $x = 40$, J: cross section at $x = 45$. All of them have the same scaling and the same number of points (2000).

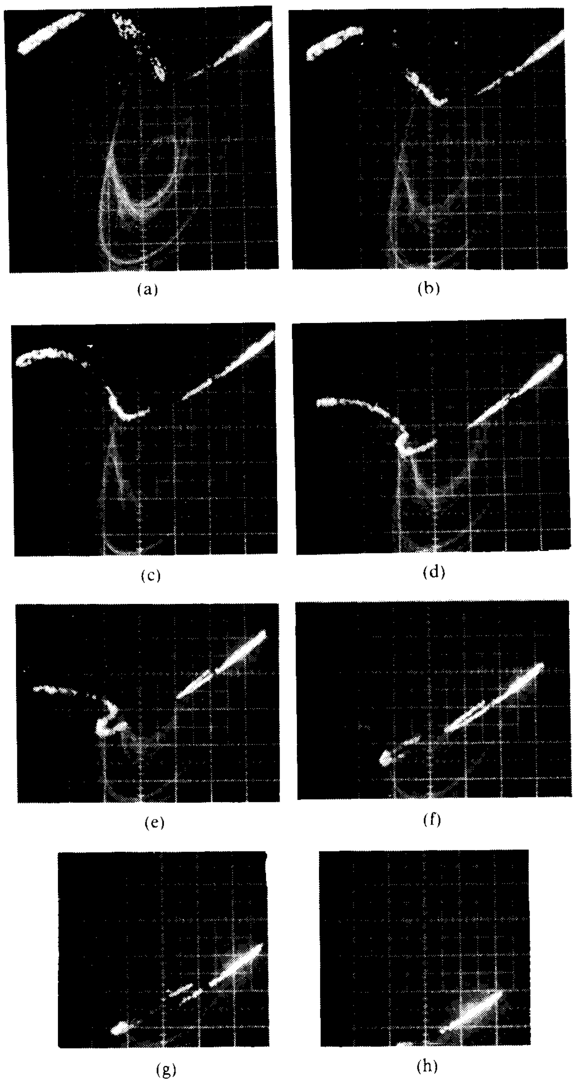

Fig. 13. Observed cross sections parallel to the (v_C, i_{L_2}) plane (corresponding to the (y, z)-plane). These pictures provide the experimental confirmation of the computer simulation of Fig. 12 (same scale for all of them). Fig. 13(a) shows the cross section for $v = 0$ (or $x = 0$), whose appearance suggests two hooks joined at their tips, hence the name "double hook" (the distortion comes from the electronic device which draws the cross sections). The following pictures illustrate the cross sections and the part of the trajectory located under the crossing plane, for increasing values for v_C (or x).

Let ϕ^t be the flow generated by (3.3) and pick an initial condition $x_0 \in E^u(P^+)$ in a neighborhood of P^+. As in the double scroll, the flow $\phi^t(x_0)$ starts wandering away from P^+ in a counterclockwise spiral and hits U_1 on L_0 (since $E^u(P^+)$ is invariant). Let x_1 be the intersection point.

If $x_1 = A$, then the trajectory goes directly to the origin (since $A \in F_{23}$, which is stable).

If $x_1 \in [AB]$, then the trajectory approaches the origin following F_{23}, but goes up again before reaching the plane $x = 0$ ($\phi^t(x_1)$ has a component on F_{23} and a component on $E^{u1}(0)$; where the latter is directed towards D_1). Going back to U_1, the flow is bounded by F_{12}, and later by F_{13}. The closer x_1 is to A, the deeper $\phi^t(x_1)$ descends. On Fig. 11 (b) the segment $[AB]$ maps into the points between B and C.

If $x_1 \in [AF]$, then the trajectory descends again towards 0, but, this time, enters the region D_{-1}.

The segment-like set of points between E and D can easily be explained as follows. Coming from D_{-1}, the flow hits U_{-1} from below, forming a segment symmetrical to $[AB]$ on U_1 with respect to the origin. As the D_0 region is very small in comparison with D_1 and D_{-1}, the previous segment is mapped into a segment-like set on U_1.

What happens to the set of points between E and D, however, remains unclear. We assume that a point G separates $[ED]$ into two parts. The first one $[EG]$ is made of points heading for P^+, meanwhile $[GD]$ is mapped into the set of points between D and C (so that the trajectory reaches D_0 again), and then into a very small region around C (probably C itself).

Fig. 12 shows various cross sections of the attractor calculated *numerically* at $x = 5k$, $k = 0$ to 9. One can observe how flat the attractor is, especially at the ends. The cross section at $x = 0$ gave the name of "double hook" to the attractor.

Fig. 13 shows the same cross sections observed in the circuit realization using the 3-D rotator described in [6]. With these cross sections we were able to observe the trajectory located under the plane of each cross section. The correspondence with the digital computations in Fig. 12 is quite remarkable.

IV. Conclusion

We have described the circuit realization of the double hook attractor, a new strange attractor using the double scroll system of equations. The double hook occurs when the eigenvalues at the origin are all *real*. We have presented experimental evidence to confirm the theoretical predictions and computer simulations of the structure of this attractor. The bifurcation sequence appears to differ considerably from the period-doubling route to chaos observed in the double scroll. Further study in this area may produce some interesting results. A comprehensive analysis of the piecewise-linear geometry and the normal form equations associated with the double hook is given in [7].

Acknowledgment

The authors would like to thank R. Tokunaga of Waseda University, Tokyo, Japan, for his very useful suggestions on the experimental work and M. P. Kennedy for his valuable comments.

References

[1] Leon O. Chua, Motomasa Komuro, and Takashi Matsumoto, "The double scroll family," *IEEE Trans. Circuits Syst.*, vol. CAS-33, pp. 1073–1118, Nov. 1986.

[2] Takashi Matsumoto, Leon O. Chua and Motomasa Komuro, "The double scroll," *IEEE Trans. Circuits Syst.*, vol. CAS-32, pp. 797–818, Aug. 1985.

[3] M. Pyee, "Fonctions et systemes electroniques," Tome 1, Ecole Nationale Superieure de l'Aeronautique et de l'Espace, Toulouse, France, 1986.

[4] Leon O. Chua and F. Ayrom, "Designing non-linear single op-amp circuits: A cook-book approach," *Int. J. Circuit Theory Appl.*, vol. 13, pp. 235–268, 1985.

[5] Leon O. Chua and Guo-Qun Zhong, "Negative resistance curve tracer," *IEEE Trans. Circuits Syst.*, vol. CAS-32, Jan. 1985.

[6] Leon O. Chua and T. Sugawara, "Panoramic view of strange attractors," *Proc. IEEE*, pp. 1107–1120, Aug. 1987.

[7] C. P. Silva and L. O. Chua, "The overdamped Double Scroll family; Part 1: Piecewise-linear geometry and normal form," *Int. J. Circuit Theory Appl.*, vol. 16, pp. 233–302, 1988.

[8] L. O. Chua, C. A. Desoer and E. S. Kuh, *Linear and Nonlinear Circuits*. New York: McGraw-Hill, 1987.

[9] S. Wu, "Chua's circuit family," *Proc. IEEE*, vol. 75, pp. 1022–1032, Aug. 1987.

Philippe Bartissol, photograph and biography not available at time of publication.

Leon O. Chua (S'60–M'62–SM'70–F'74), for photograph and biography please see page 880 of the July 1988 issue of this TRANSACTIONS.